Magnetic resonance induced pseudoelectric field and giant current response in axion insulators

Jiabin Yu,[1] Jiadong Zang,[2] and Chao-Xing Liu[1,*]

[1]*Department of Physics, Pennsylvania State University, University Park, Pennsylvania 16802, USA*
[2]*Department of Physics and Astronomy, University of New Hampshire, Durham, New Hampshire 03824, USA*

A quantized version of the magnetoelectric effect, known as the topological magnetoelectric effect, can exist in a time-reversal invariant topological insulator with all its surface states gapped out by magnetism. This topological phase, called the axion insulator phase, has been theoretically proposed but still lacks conclusive experimental evidence due to the small signal of topological magnetoelectric effect. In this work, we propose that the dynamical in-plane magnetization in an axion insulator can generate a pseudoelectric field, which acts on the surface state of topological insulator films and leads to the nonzero response current. Strikingly, we find that the current at magnetic resonance (either ferromagnetic or antiferromagnetic) is larger than that of topological magnetoelectric effect by several orders of magnitude and thereby serves as evidence to confirm the axion insulator phase in the candidate materials.

I. INTRODUCTION

More than 40 years ago, the axion was proposed as an elementary particle to resolve the strong CP problem in high-energy physics [1–4]. Later studies suggested that the axion might be a candidate for the dark matter in the universe [5–8]. While axions so far remain experimentally elusive, it has been proposed that the electrodynamics of axions [9] may effectively exist in a variety of solid-state systems, in particular the system based on the topological insulator (TI) [10–12]. In contrast to the conventional Maxwell's equations for a trivial insulator, the electromagnetic response in the bulk of TIs requires an additional term (known as the θ term) in the action:

$$S_\theta = \frac{e^2}{hc} \int dt d^3 r \frac{\theta}{2\pi} \boldsymbol{E} \cdot \boldsymbol{B}, \tag{1}$$

where e is the elementary charge and θ is the dimensionless pseudoscaler axion field. If time-reversal (TR) symmetry is preserved, θ can only take two topologically distinct values in the bulk of a system: 0 for a trivial insulator and π for a TI. The gauge transformation can change the value of θ by $2\pi n$ with n an arbitrary integer without affecting the bulk topology, reflecting the Z_2 topological classification. As a consequence, gapless modes must exist at the interface between a TI and a trivial insulator (or the vacuum) in the presence of TR symmetry, as θ cannot vary continuously without gap closing or TR-breaking effects [12]. This topological surface state leads to a variety of exotic phenomena in TI materials, including the quantum anomalous Hall (QAH) effect [13], the topological magneto-optical effect [14–16] even with exact quantization in terms of fine-structure constant [14], topological magnetoelectric effect (TME) [12,17], and the image magnetic monopole [18].

When *all* the surface modes of a TR-invariant TI are gapped out by the surface magnetic coating with a hedge-hog magnetization configuration, the $2\pi n$ ambiguity can be removed and the θ value is uniquely determined [12,17–20]. This system with a well-defined nonzero θ field in Eq. (1) is defined as the axion insulator (AI) [17,21,22]. The polarization (magnetization) of an AI can be induced by a magnetic (electric) field in the same direction with the response coefficient quantized to $\frac{\theta e^2}{2\pi hc}$ [12,17], serving as a conclusive experimental signature to distinguish an AI from a trivial insulator. Such effect is called TME and requires θ to be well defined everywhere in the system since θ determines the experimentally measurable magnetoelectric coefficient. Besides the unique TME, the AI also exhibits the zero Hall resistance with large longitudinal resistance, which is nevertheless not conclusive since it can also happen in trivial insulators. The AI phase has been proposed in the ferromagnetic insulator-TI-ferromagnetic insulator (FMI-TI-FMI) heterostructure [17,21,22], antiferromagnetic topological insulator $MnBi_2Te_4$ [23–26], and various other materials [27–31]. Although the zero Hall plateau has been observed in the FMI-TI-FMI heterostructure [21,22], the conclusive TME has not been detected due to the small magnetoelectric current. Therefore, identifying a testable transport signal to distinguish the AI from a trivial insulator is the major challenge of the field.

In this paper, we propose that the magnetic resonance (MR) in an AI can induce a pseudoelectric field (PEF), leading to a response current which is much larger than that of TME. This current response cannot exist in a trivial insulator and thus serves as a feasible and unequivocal experimental evidence to identify the AI phase. Moreover, our proposal serves as the first concrete example of MR-induced PEF in realistic materials. The intuitive picture is summarized in Fig. 1, which takes FMI-TI-FMI heterostructure as an example. In the FMI-TI-FMI heterostructure, the QAH state can exist when the two FMIs have parallel magnetic moments [Figs. 1(b)
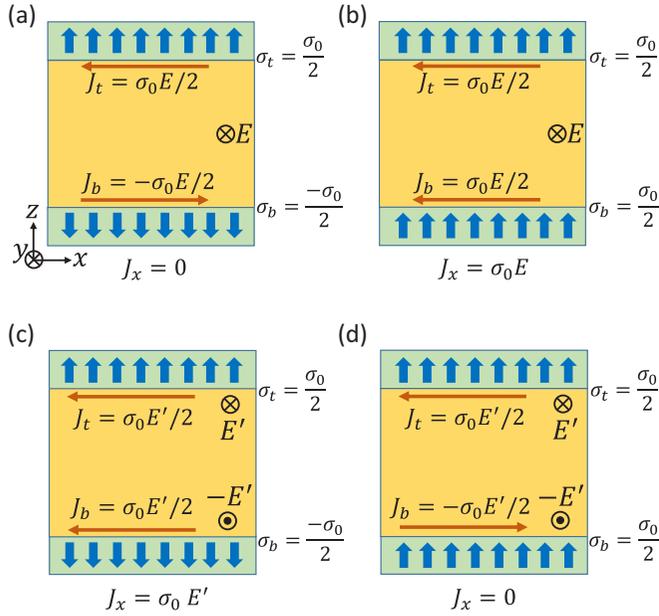
FIG. 1. In the four graphs, the yellow middle parts are TIs and the green parts are FMIs with blue arrows the magnetization. Panels (a) and (c) are AIs with opposite surface Hall conductance $\sigma_t = -\sigma_b$, and panels (b) and (d) are QAH insulators with $\sigma_t = \sigma_b$. In the uniform electric field E along y, the AI in panel (a) has zero total Hall current ($J_x = 0$) due to the opposite surface Hall currents ($J_t = -J_b$), while the QAH insulator in panel (b) has nonzero Hall current with Hall conductance $\sigma_0 = -e^2/h$. If the electric field E' is in opposite y directions on the two surfaces, AI in panel (c) has nonzero Hall current, but the QAH insulator in panel (d) has zero Hall current.

and 1(d)], while the AI phase is expected for the antiparallel configuration [Figs. 1(a) and 1(c)]. The TI surface states open a gap due to magnetic proximity and show half quantized Hall conductance with its sign depending on the magnetization direction. With a uniform electric field, the Hall currents of the top and bottom surfaces have the same direction in the QAH phase [Fig. 1(b)] but cancel each other in Fig. 1(a), leading to the zero Hall plateau of the AI phase. However, the zero Hall plateau may also occur in a trivial or Anderson insulator [32–35]. In contrast, for an in-plane electric field with opposite directions at two surfaces, the Hall current is expected to be nonzero in the AI phase [Fig. 1(c)] but vanishes for the QAH state [Fig. 1(d)]. As a direct consequence of TME in AIs [17], the nonuniform electric field and the resultant current response in Fig. 1(c) can be generated by a time-dependent magnetic field, but the current magnitude is limited by the TI film thickness (maximally tens of nanometers). Instead of electric fields, we consider the dynamics of in-plane magnetization in the FMI layers. The in-plane magnetization acts on the TI surface states effectively as a time-dependent pseudogauge field (PGF) [36], and thus generates a PEF of the same form as the physical electric field in Figs. 1(c) and 1(d), leading to nonzero current response in the AI phase. In particular, our estimation shows that the current induced by the PEF at ferromagnetic resonance (FMR) in the heterostructures (or the antiferromagnetic resonance (AFMR) in the MnBi$_2$Te$_4$ system) is giant.

II. PEF INDUCED BY DYNAMICAL IN-PLANE MAGNETIZATION

We start from demonstrating that the dynamical in-plane magnetization of the FMIs in Fig. 1 can induce the PEF and the current response. The low-energy physics of the FMI-TI-FMI heterostructure is given by the surface states of the TI film coupled to surface magnetization and the external electromagnetic field, resulting in the following Hamiltonian [37]:

$$H = \int \frac{d^2k}{(2\pi)^2} \sum_i c_{\boldsymbol{k},i}^\dagger [h_{0,i} + h_Z + h_{ex,i}] c_{\boldsymbol{k},i}. \quad (2)$$

The equation

$$h_{0,i} = v_{f,i}\left[-\sigma_y\left(\hbar k_x + \frac{e}{c}A_{i,x}\right) + \sigma_x\left(\hbar k_y + \frac{e}{c}A_{i,y}\right)\right] + (-e)\varphi_i \quad (3)$$

depicts the surface Dirac modes $c_{\boldsymbol{k},i}^\dagger = (c_{\boldsymbol{k},i,\uparrow}^\dagger, c_{\boldsymbol{k},i,\downarrow}^\dagger)$ coupled to the 2+1D physical gauge field $A_i^\mu = (\varphi_i, A_{i,x}, A_{i,y})$, where $i = t, b$ labels the top and bottom surfaces, respectively, $\boldsymbol{k} = (k_x, k_y)$, $v_{f,t} = -v_{f,b} = v_f$, and $\sigma_{x,y,z}$ are Pauli matrices for spin. $h_Z = \mu_B \boldsymbol{B} \cdot \boldsymbol{\sigma}$ is the Zeeman term with μ_B Bohr magneton and $\boldsymbol{B}$ the uniform magnetic field, and $h_{ex} = g_M \boldsymbol{M}_i \cdot \boldsymbol{\sigma}$ is the exchange coupling term with g_M assumed to be positive and the same on both surfaces for simplicity. We notice that the in-plane components of the Zeeman and exchange coupling terms play the same role as the vector potential and thus can be regarded as the PGF. For convenience, we transform the creation operator to the Grassmann field $\bar{\psi}_i$ and rewrite the Hamiltonian into the action form

$$S = \int d^3x\, \bar{\psi}_i\left[\Gamma_i^\mu\left(i\hbar\partial_\mu - \frac{e}{c}\widetilde{A}_{i,\mu}\right) - \frac{m_{i,z}}{c}\sigma_z\right]\psi_i, \quad (4)$$

where $x^\mu = (ct, x, y)$ and $\Gamma_i^\mu = (1, -\frac{v_{f,i}}{c}\sigma_y, \frac{v_{f,i}}{c}\sigma_x)$. In Eq. (4), $m_{i,z}$ plays the role of mass, and $\widetilde{A}_{i,\mu} = A_{i,\mu} + A_{i,\mu}^{pse}$ contains the PGF,

$$A_{i,\mu}^{\text{pse}} = \frac{c}{ev_{f,i}}(0, -m_{i,y}, m_{i,x}), \quad (5)$$

where $\boldsymbol{m}_i = \mu_B \boldsymbol{B} + g_M \boldsymbol{M}_i$. The corresponding "electric" field of $\widetilde{A}_{i,\mu}$ can be written as $\widetilde{E}_{i,a} = -\partial_a\varphi_i - \frac{1}{c}\frac{\partial \widetilde{A}_{i,a}}{\partial t} = E_{i,a} + E_{i,a}^{pse}$ with $E_{i,a}$ being the conventional electric field and $a = x, y$. We call $E_{i,a}^{pse} = \frac{1}{ev_{f,i}}(\dot{m}_{i,y}, -\dot{m}_{i,x})$ the PEF, following the terminology used for pseudomagnetic field induced by strain in graphene [38]. Next, we derive the response current generated by PEF based on Eq. (4).

By integrating out the fermionic modes in Eq. (4), the response of the system to the leading order can be obtained,

$$J_i^\mu = \sigma_i \varepsilon^{\mu\rho\nu}\partial_\rho \widetilde{A}_{i,\nu}, \quad (6)$$

where $J_i^\mu = (c\rho_i, J_i^x, J_i^y)$ is the current density of i surface and $\partial_\rho = \partial_{x^\rho}$. Then,

$$\sigma_i = -\text{sgn}(m_{i,z})\frac{e^2}{2h} \quad (7)$$

is the Hall conductance of i surface, showing that the surface Hall conductance is determined by the sign of the surface gap. We now focus on the AI phase with antiparallel magnetization

alignment. As the exchange coupling is generally much larger than Zeeman coupling ($|g_M M_{i,z}| \gg |\mu_B B_z|$), we expect opposite Hall conductance on two surfaces ($\sigma_b = -\sigma_t$). Therefore, the total current density depends on only the difference between $\widetilde{A}_t$ and $\widetilde{A}_b$ as

$$J_{AP}^{\mu} = \sigma_t \varepsilon^{\mu\rho\nu} \partial_\rho (\widetilde{A}_{t,\nu} - \widetilde{A}_{b,\nu}). \tag{8}$$

Thus, the PEF can induce currents in the same way as the physical electric field according to $\varepsilon^{\mu\rho\nu} \partial_\rho \widetilde{A}_{i,\nu} = (\widetilde{B}_{i,z}, \widetilde{E}_{i,y}, -\widetilde{E}_{i,x})$, and the physics in Figs. 1(a) and 1(c) can be described by Eq. (8) if choosing $E = (\widetilde{E}_{t,y} + \widetilde{E}_{b,y})/2$ and $E' = (\widetilde{E}_{t,y} - \widetilde{E}_{b,y})/2$. In the following, we consider a simple case where the uniform magnetic field only has an oscillating x component, i.e., $\boldsymbol{B}(t) = [B_0 \cos(\omega t), 0, 0]$ with the constant B_0, in order to estimate the current magnitude.

The oscillating uniform magnetic field can induce a nonuniform electric field along y owing to Faraday's law, $E_y(t,z) = -\omega B_0 \sin(\omega t)z/c$, with $z = 0$ set at the middle of the TI layer. In this case, the physical gauge field in Eq. (4) must satisfy $\varepsilon^{1\rho\nu}\partial_\rho A_{i,\nu} = E_y(t,z_i) = -\omega B_0 \sin(\omega t)z_i/c$, where $z_{t(b)} = (-)L_z/2$ and L_z is the distance between two surfaces. In addition, $\boldsymbol{B}$ can also drive the surface magnetic moments away from the z direction and thus induce the time-dependent in-plane magnetization $M_{i,a}$. In sum, under the adiabatic approximation $\hbar\omega \ll |g_s M_{i,z}|$, we have

$$J_{AP}^x = J_E + J_Z + J_M, \tag{9}$$

for the antiparallel case. In the above equation, $J_E = -\frac{1}{c}\sigma_t B_0 \omega \sin(\omega t)L_z$ is the TME current density, $J_Z = 2\sigma_t E_Z^{pse}$ with $E_Z^{pse} = \frac{1}{ev_f}\mu_B B_0 \omega \sin(\omega t)$ is the PEF induced by the in-plane Zeeman term, and $J_M = 2\sigma_t E_M^{pse}$ with $E_M^{pse} = -\frac{1}{2ev_f}g_M(\dot{M}_{t,x} + \dot{M}_{b,x})$. Among these contributions, let us first estimate J_E and J_Z. With typical values of parameters $L_z = 20$ nm, $v_f = 6.5 \times 10^5$ m/s, $B_0 = 10$ G, and $L_y = 200$ μm (the length of the sample along y) [26], the current amplitude of TME is estimated as (after converting to SI units) $I_E = |\max(J_E)L_y| = 0.5(\frac{\omega}{2\pi \text{GHz}})$nA, which is small for GHz frequency. On the other hand, the current induced by the Zeeman effect can be neglected as $|J_Z/J_E| \approx 9 \times 10^{-3}$. In the next section, we focus on the current response generated by the magnetization-induced PEF, i.e., J_M.

III. FMR IN FMI-TI-FMI HETEROSTRUCTURES

In the FMI-TI-FMI heterostructure, the in-plane magnetization and the induced current are maximized at the FMR frequency of the FMI layer. Since two FMI layers are decoupled by the TI layer, the Landau-Lifshitz-Gilbert (LLG) equations [39–41] for two FMI layers under the same uniform magnetic field $\boldsymbol{B}(t)$ have the same form and can be treated separately. The equation is solved in the limit that the second and higher order terms of $|M_{i,x}|/|\boldsymbol{M}_i|$, $|M_{i,y}|/|\boldsymbol{M}_i|$, and $|B_0|/|\boldsymbol{M}_i|$ are small enough to be neglected, and the steady solution of $M_{i,x}$ at FMR is given by

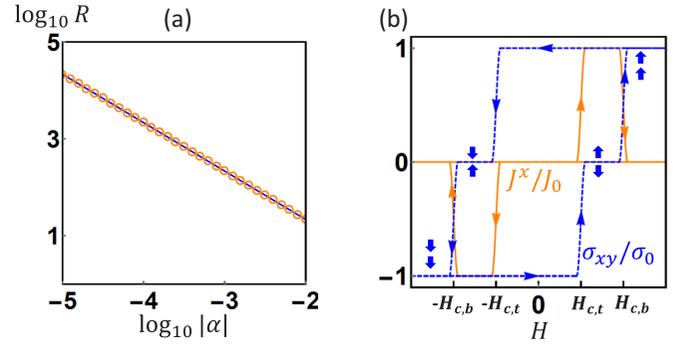$$M_{i,x} = \frac{\gamma_0 B_0 M_s}{2\alpha\omega_0}\sin(\omega_0 t), \tag{10}$$

FIG. 2. Panel (a) shows how the ratio between the FMR-induced and TME currents, noted as R, changes with the damping constant α. The orange circle (blue line) is given by the solution of LLG equation with (without) higher order terms of α. Panel (b) schematically shows how the FMR-induced AC current density along x (J^x in orange) and the total DC Hall conductance σ_{xy} (blue) change with the initializing magnetic field H along z. Here, the setup considered is shown in Fig. 1 and the current is measured after decreasing H to guarantee FMR on both surfaces. The on-line arrows indicate the direction of changing H, while the vertical off-line blue arrows imply the magnetization configuration at the corresponding plateau of the blue line. J_0 is the postfactor of $\text{sgn}(M_{t,z})$ in Eq. (11).

where α is the dimensionless damping constant, $M_s = |\boldsymbol{M}_i|$ is the magnetization amplitude, ω_0 is resonance frequency, and $\gamma_0 = 2e/(2m_e c)$ is the magnetomechanical ratio of electrons (see Sec. B in Ref. [42]). In the derivation of the above expression, we assume the same magnetization amplitude, resonant frequency, and damping constant for two FMIs, and only keep the leading order term of α. Since two FMIs are driven by the same uniform magnetic field, $M_{t,x}$ and $M_{b,x}$ have the same sign in Eq. (10). The typical FMR frequency is $\omega_0 = 2\pi$ GHz, and its energy scale $\hbar\omega_0 \approx 4$ μeV is much smaller than the magnetic gap of the FMI ($|g_M M_s| = 0.1$ meV) [22]. Thus, the adiabatic approximation holds, and we can combine Eq. (10) with Eq. (9) to get the current density induced by magnetic dynamics at the FMR:

$$J_M = \text{sgn}(M_{t,z})\frac{eB_0\gamma_0 g_M M_s}{2v_f h\alpha}\cos(\omega_0 t). \tag{11}$$

Then the ratio between the amplitudes of J_M and J_E is

$$R = \left|\frac{\max(J_M)}{\max(J_E)}\right| = \left|\frac{\hbar/L_z}{m_e v_f}\right|\left|\frac{g_M M_s}{\hbar\omega_0}\right|\frac{1}{|\alpha|} \approx \frac{0.2}{|\alpha|} \tag{12}$$

with the TME current $I_E = 0.5$ nA. Although the above equation is obtained by neglecting higher order terms of α, the approximation is quite good, as shown in Fig. 2(a). In a typical range $|\alpha| = 10^{-5}$–10^{-2} for FMIs [43], the ratio is approximately $R \approx 20$–2×10^4, resulting in the experimentally measurable current amplitude $I_M = I_E R \approx 10$–10^4 nA. Therefore, the current response induced by magnetic dynamics at FMR is the dominant contribution, i.e., $J_{AP}^x \approx J_M$ for Eq. (9), and can be used to distinguish the AI from a trivial insulator experimentally.

We next compare the current response induced by FMR to the standard DC Hall conductance in the FMI-TI-FMI heterostructures when varying initializing magnetic fields.

Experimentally, the FMI-TI-FMI heterostructure is realized by inserting a TI layer between a Cr-doped TI layer (top) and a V-doped TI layer (bottom) [22]. Since the coercive field $H_{c,t}$ of Cr-doped layer is around 0.14T, much smaller than $H_{c,b} \sim 1$T of V-doped layer, a two-step transition of Hall conductance, schematically shown by the dashed blue line in Fig. 2(b), has been demonstrated in experiments (see Fig. 2 in Ref. [22]). The AI phase is expected to exist when the Hall conductance is zero with antiparallel magnetization at two surfaces in the intermediate field ranges $-H_{c,b} < H < -H_{c,t}$ and $H_{c,t} < H < H_{c,b}$. When the state with zero Hall conductance is achieved, the mechanism discussed here will induce a large current response at the FMR frequency. We emphasize that the initializing magnetic field should be reduced or removed before measuring the current response of FMR to guarantee a similar FMR frequency of two FMI layers [44]. On the other hand, when the DC transport measurement shows a QAH state with Hall conductance $\sigma_{xy} = \pm e^2/h$, the current response at the FMR frequency is expected to be quite small owing to the opposite directions of FMR-induced PEFs on the two surfaces [42]. The behaviors of DC transport and the current measurement at the FMR frequency are schematically shown in Fig. 2(b), and the sharp contrast between these two measurements can serve as the key evidence of AI phase.

IV. AFMR IN MnBi$_2$Te$_4$

MnBi$_2$Te$_4$ has A-type antiferromagnetism (AFM): Ferromagnetic layers with opposite out-of-plane magnetization are alternatively stacked along the z direction. Because of the combined symmetry of half translation and TR for AFM, the bulk Hamiltonian of MnBi$_2$Te$_4$ is the same as the TI Hamiltonian of Bi$_2$Te$_3$ [26]. The topological surface states on both surfaces are gapped by ferromagnetic layers, resulting in the fact that the low-energy action of MnBi$_2$Te$_4$ has the same form as Eq. (4). Because of the intrinsic magnetism in MnBi$_2$Te$_4$, the exchange coupling between surface electrons and magnetization is much stronger than that of the proximity effect in the FMI-TI-FMI heterostructure and leads to a larger magnetic gap ($g_M M_s \approx 0.1$ eV) of surface states [23–26]. In the following, we consider an even number of layers of MnBi$_2$Te$_4$ films so that the top and bottom layers have antiparallel magnetization. To describe the magnetic dynamics of AFM in MnBi$_2$Te$_4$, particularly around the AFMR, the exchange interaction of magnetization between the neighboring layers should be included in the LLG equation and leads to a larger resonance frequency $\omega_1 \sim$ THz [45–47]. Since 0.1 eV $\gg h$ (1 THz) ≈ 4 meV, the adiabatic approximation is still valid and Eq. (9) can be applied in this case.

The LLG equation for this AFM system can be solved with the same approximation as the FMR case, and the steady solution at AFMR reads

$$M_{i,x} = \frac{\gamma_0 B_0 M_s}{2\alpha\omega_1} \frac{B_A}{B_A + B_E} \sin(\omega_1 t), \quad (13)$$

where B_E and B_A are the exchange field and anisotropy field, respectively. (See details in Sec. C of Ref. [42]). The resulting current J_M from Eq. (13) is derived as

$$J_M = \text{sgn}(M_{t,z}) \frac{e B_0 \gamma_0 g_M M_s}{2 v_f h \alpha} \frac{B_A}{B_A + B_E} \cos(\omega_1 t). \quad (14)$$

By choosing $g_M M_s = 0.1$ eV, $\omega_1 = 2\pi$ THz, and all other parameters to be the same as in the FMR case, we find that the current J_Z induced by Zeeman coupling is still negligible, while the TME current amplitude becomes $I_E = 500$ nA owing to the increase of the resonance frequency. The ratio between the amplitudes of J_M and J_E now reads

$$R = \left| \frac{\max(J_M)}{\max(J_E)} \right| = \left| \frac{\hbar/L_z}{m_e v_f} \frac{g_M M_s}{\hbar\omega_1} \frac{B_A}{B_A + B_E} \right| \frac{1}{|\alpha|} \approx \frac{0.2}{|\widetilde{\alpha}|}, \quad (15)$$

where $\widetilde{\alpha} = \alpha(B_A + B_E)/B_A$. By choosing a typical ratio between the exchange and anisotropy fields $|B_E/B_A| = 10^2$ [46] and the same typical range of $|\alpha|$ as the FMR case, we find $R \approx 0.2$–200. Thus, the AFMR-induced current may still be dominated when $|\alpha|$ can be reduced, and its amplitude ($I_M \approx 0.1$–100 μA) is much larger than the FMR case. Since the magnetization along x has the same form on two surfaces according to Eq. (13), the AFMR-induced current in the QAHI phase (odd number of layers) of MnBi$_2$Te$_4$ is zero, similar to that in the FMR case. This suggests an even-odd effect of the AFMR-induced current response in MnBi$_2$Te$_4$ films due to different surface magnetization configurations.

V. CONCLUSION AND DISCUSSION

In summary, we have demonstrated that magnetic dynamics in the FMI-TI-FMI heterostructure and MnBi$_2$Te$_4$ can give rise to PEF, which in turn generates a giant current response at the FMR or AFMR in AIs but not in trivial insulators or QAH insulators. Given the observation of zero Hall plateau [21,22], this phenomenon awaits an experimental test in FMI-TI-FMI heterostructure. Current experiments on MnBi$_2$Te$_4$ films have shown heavy electron doping [23], which is detrimental to the mechanism proposed here. Therefore, an electric gate is required on MnBi$_2$Te$_4$ films and our theory predicts that the AFMR-induced current response will be greatly enhanced when the Fermi energy is gated into the magnetic gap. Although the PEF has been studied in graphene with the dynamical strain [48], our proposal of MR-induced PEF is more feasible since MR has been observed and studied since the 1940s [39,49,50]. Our AFMR-induced current has a fundamentally different mechanism from that induced by the bulk dynamical axion field discussed in Refs. [27,51], as the latter requires a nonzero external static magnetic field that is absent in our proposal. Our theory unveils the intriguing interplay between magnetic dynamics and magnetoelectric response in the AI phase and will pave the way to a new class of electric-field-tunable axion devices for spintronics applications [52].

[1] R. D. Peccei and H. R. Quinn, Phys. Rev. Lett. **38**, 1440 (1977).

[2] R. D. Peccei and H. R. Quinn, Phys. Rev. D **16**, 1791 (1977).

[3] S. Weinberg, Phys. Rev. Lett. **40**, 223 (1978).

[4] F. Wilczek, Phys. Rev. Lett. **40**, 279 (1978).

[5] J. Preskill, M. B. Wise, and F. Wilczek, Phys. Lett. B **120**, 127 (1983).

[6] L. Abbott and P. Sikivie, Phys. Lett. B **120**, 133 (1983).

[7] M. Dine and W. Fischler, Phys. Lett. B **120**, 137 (1983).

[8] J. Ipser and P. Sikivie, Phys. Rev. Lett. **50**, 925 (1983).

[9] F. Wilczek, Phys. Rev. Lett. **58**, 1799 (1987).

[10] M. Z. Hasan and C. L. Kane, Rev. Mod. Phys. **82**, 3045 (2010).

[11] X.-L. Qi and S.-C. Zhang, Rev. Mod. Phys. **83**, 1057 (2011).

[12] X.-L. Qi, T. L. Hughes, and S.-C. Zhang, Phys. Rev. B **78**, 195424 (2008).

[13] C.-Z. Chang, J. Zhang, X. Feng, J. Shen, Z. Zhang, M. Guo, K. Li, Y. Ou, P. Wei, L.-L. Wang *et al.*, Science **340**, 167 (2013).

[14] L. Wu, M. Salehi, N. Koirala, J. Moon, S. Oh, and N. Armitage, Science **354**, 1124 (2016).

[15] V. Dziom, A. Shuvaev, A. Pimenov, G. Astakhov, C. Ames, K. Bendias, J. Böttcher, G. Tkachov, E. Hankiewicz, C. Brüne *et al.*, Nat. Commun. **8**, 15197 (2017).

[16] K. N. Okada, Y. Takahashi, M. Mogi, R. Yoshimi, A. Tsukazaki, K. S. Takahashi, N. Ogawa, M. Kawasaki, and Y. Tokura, Nat. Commun. **7**, 12245 (2016).

[17] J. Wang, B. Lian, X.-L. Qi, and S.-C. Zhang, Phys. Rev. B **92**, 081107 (2015).

[18] X.-L. Qi, R. Li, J. Zang, and S.-C. Zhang, Science **323**, 1184 (2009).

[19] A. M. Essin, J. E. Moore, and D. Vanderbilt, Phys. Rev. Lett. **102**, 146805 (2009).

[20] T. Morimoto, A. Furusaki, and N. Nagaosa, Phys. Rev. B **92**, 085113 (2015).

[21] M. Mogi, M. Kawamura, A. Tsukazaki, R. Yoshimi, K. S. Takahashi, M. Kawasaki, and Y. Tokura, Sci. Adv. **3**, eaao1669 (2017).

[22] D. Xiao, J. Jiang, J.-H. Shin, W. Wang, F. Wang, Y.-F. Zhao, C. Liu, W. Wu, M. H. W. Chan, N. Samarth, and C.-Z. Chang, Phys. Rev. Lett. **120**, 056801 (2018).

[23] M. M. Otrokov, I. I. Klimovskikh, H. Bentmann, A. Zeugner, Z. S. Aliev, S. Gass, A. U. Wolter, A. V. Koroleva, D. Estyunin, A. M. Shikin *et al.*, arXiv:1809.07389.

[24] Y. Gong, J. Guo, J. Li, K. Zhu, M. Liao, X. Liu, Q. Zhang, L. Gu, L. Tang, X. Feng *et al.*, Chin. Phys. Lett. **36**, 076801 (2019).

[25] J. Li, Y. Li, S. Du, Z. Wang, B.-L. Gu, S.-C. Zhang, K. He, W. Duan, and Y. Xu, Sci. Adv. **5**, eaaw5685 (2019).

[26] D. Zhang, M. Shi, K. He, D. Xing, H. Zhang, and J. Wang, Phys. Rev. Lett. **122**, 206401 (2019).

[27] R. Li, J. Wang, X.-L. Qi, and S.-C. Zhang, Nat. Phys. **6**, 284 (2010).

[28] M. Mogi, M. Kawamura, R. Yoshimi, A. Tsukazaki, Y. Kozuka, N. Shirakawa, K. Takahashi, M. Kawasaki, and Y. Tokura, Nat. Mater. **16**, 516 (2017).

[29] S. Chowdhury, K. F. Garrity, and F. Tavazza, npj Comp. Mat. **5**, 33 (2019).

[30] X. Gui, I. Pletikosic, H. Cao, H.-J. Tien, X. Xu, R. Zhong, G. Wang, T.-R. Chang, S. Jia, T. Valla *et al.*, arXiv:1903.03888.

[31] Y. Xu, Z. Song, Z. Wang, H. Weng, and X. Dai, Phys. Rev. Lett. **122**, 256402 (2019).

[32] Y. Feng, X. Feng, Y. Ou, J. Wang, C. Liu, L. Zhang, D. Zhao, G. Jiang, S.-C. Zhang, K. He *et al.*, Phys. Rev. Lett. **115**, 126801 (2015).

[33] J. Wang, B. Lian, and S.-C. Zhang, Phys. Rev. B **89**, 085106 (2014).

[34] C.-Z. Chang, W. Zhao, J. Li, J. K. Jain, C. Liu, J. S. Moodera, and M. H. W. Chan, Phys. Rev. Lett. **117**, 126802 (2016).

[35] C.-Z. Chen, H. Liu, and X. C. Xie, Phys. Rev. Lett. **122**, 026601 (2019).

[36] A. Iorio and P. Pais, Phys. Rev. D **92**, 125005 (2015).

[37] I. Garate and M. Franz, Phys. Rev. Lett. **104**, 146802 (2010).

[38] N. Levy, S. A. Burke, K. L. Meaker, M. Panlasigui, A. Zettl, F. Guinea, A. H. C. Neto, and M. F. Crommie, Science **329**, 544 (2010).

[39] C. Kittel, Phys. Rev. **73**, 155 (1948).

[40] C. Kittel, *Introduction to Solid State Physics* (Wiley New York, 1976), Vol. 8.

[41] A. Aharoni, *Introduction to the Theory of Ferromagnetism*, International Series of Monographs on Physics (Oxford University Press, New York, USA, 2000), Vol. 109.

[42] See Supplemental Material at http://link.aps.org/supplemental/10.1103/PhysRevB.100.075303 for details on the linear response, FMR, and AFMR.

[43] C. Hauser, T. Richter, N. Homonnay, C. Eisenschmidt, M. Qaid, H. Deniz, D. Hesse, M. Sawicki, S. G. Ebbinghaus, and G. Schmidt, Sci. Rep. **6**, 20827 (2016).

[44] It is because the initializing field H can change the resonant frequencies of two FMIs [39]. If two FMIs have the same (slightly different) zero-field resonant frequencies, H should be reduced to zero (a small nonzero value to compensate the difference) before measuring the FMR-induced current.

[45] C. Kittel, Phys. Rev. **82**, 565 (1951).

[46] F. Keffer and C. Kittel, Phys. Rev. **85**, 329 (1952).

[47] Z. Wang, S. Kovalev, N. Awari, M. Chen, S. Germanskiy, B. Green, J.-C. Deinert, T. Kampfrath, J. Milano, and M. Gensch, Appl. Phys. Lett. **112**, 252404 (2018).

[48] A. Vaezi, N. Abedpour, R. Asgari, A. Cortijo, and M. A. H. Vozmediano, Phys. Rev. B **88**, 125406 (2013).

[49] J. Griffiths, Nature (London) **158**, 670 (1946).

[50] W. A. Yager and R. M. Bozorth, Phys. Rev. **72**, 80 (1947).

[51] A. Sekine and K. Nomura, Phys. Rev. Lett. **116**, 096401 (2016).

[52] A. Sekine and T. Chiba, Phys. Rev. B **93**, 220403 (2016).